J. Marine Sci. Appl. (2016) 15: 136-143
DOI: 10.1007/s11804-016-1357-7

Mathematical Model for Takeoff Simulation of a Wing in Proximity to the Ground

Omer Kemal Kinaci*

Naval Architecture and Maritime Faculty, Yildiz Technical University, Istanbul 34349, Turkey

Abstract: Aircraft flying close to the ground benefit from enhanced efficiency owing to decreased induced drag and increased lift. In this study, a mathematical model is developed to simulate the takeoff of a wing near the ground using an Iterative Boundary Element Method (IBEM) and the finite difference scheme. Two stand-alone sub-codes and a mother code, which enables communication between the sub-codes, are developed to solve for the self-excitation of the Wing-In-Ground (WIG) effect. The aerodynamic force exerted on the wing is calculated by the first sub-code using the IBEM, and the vertical displacement of the wing is calculated by the second sub-code using the finite difference scheme. The mother code commands the two sub-codes and can solve for the aerodynamics of the wing and operating height within seconds. The developed code system is used to solve for the force, velocity, and displacement of an NACA6409 wing at a 4° Angle of Attack (AoA) which has various numerical and experimental studies in the literature. The effects of thickness and AoA are then investigated and conclusions were drawn with respect to generated results. The proposed model provides a practical method for understanding the flight dynamics and it is specifically beneficial at the pre-design stages of a WIG effect craft.

Keywords: wing-in-ground effect, ground proximity, flight dynamics, iterative boundary element method, mathematical model, takeoff simulation

Article ID: 1671-9433(2016)02-0136-08

1 Introduction

Wing-in-ground (WIG) craft are "efficient" airplanes that have enhanced lift-to-drag ratios. The ground restrains the formation of tip vortices at the ends of the wings, lowering induced drag and trapping air under the wings to increase lift, reduce fuel consumption, and increase cargo weight. WIG craft are fast and can use water as a natural runway. The benefits of flying close to the ground were first exploited by Russians during the Cold War (Rozhdestvensky, 2006). Although initial excitement disappeared after several accidents, interest in WIG craft appears to be on the rise again as a result of recent breakthroughs in control engineering (Halloran and O'Meara, 1999).

WIG craft are much faster than conventional aircraft and do not require a runway when they operate over water. However, operating waters should be predefined during the design stage. Wave height and obstacles such as bridges or offshore platforms in target waters should be known beforehand to ensure that operational parameters can be calculated accordingly. A coastal map may also be important if the craft is to reach given altitudes to avoid obstacles such as mountains or sea cliffs. To resolve any issues related to the safety of the craft, it is beneficial to simulate takeoff and specify the operating height.

The production of a vehicle as complex as a WIG craft requires a design spiral with many iterations. Rough estimation of the takeoff and operational height during the pre-design stage increases the efficiency of the design process and decreases the number of iterations needed for the design spiral. The use of commercial Computational Fluid Dynamics (CFD) programs for solving Reynolds-Averaged Navier–Stokes Equations (RANSEs) may help in observing the flow physics during the late stages of the design spiral because it is not possible to try every possible wing geometry given the time required to setup a mesh system. This study attempts to utilize the practicality of the Iterative Boundary Element Method (IBEM) to quickly determine the basics of the dynamics of the WIG effect. The implemented method returns results very quickly. The IBEM is a robust method used in many fields of engineering, in particular, fluid mechanics, where it is used to solve various problems such as cavitation (Kinnas and Fine, 1993) and the free-surface effect (Bal and Kinnas, 2002; Uslu and Bal, 2008).

Although water may provide a natural runway for WIG craft, the scope of the present study is limited to the ground with solid boundaries because the effect of a free fluid surface that serves as the ground under a wing is negligible. Liang and Zong (2011) investigated differences between the effects of solid boundaries and free water surfaces on a wing. The free-surface deformation of a WIG was studied numerically using CFD by Barber (2007). Overall, these studies can be used to obtain a deeper understanding of the free-surface effect on a wing.

Flying very close to the ground can cause a wing to oscillate and produce wake vorticity, significantly affecting the longitudinal stability of a WIG craft (Nebylov, 2003).

Received date: 2015-11-10
Accepted date: 2015-11-18
Foundation item: Supported by Yildiz Technical University Scientific Research Projects Coordination Department under Project No. 2013-10-01-KAP02
***Corresponding author Email:** kemalkinaci@gmail.com; kinaci@yildiz.edu.tr

Longitudinal stability and control of the craft are the most important design parameters (Yang *et al*., 2015) when a wing is under extreme ground effects. An exemplary study carried out for a small passenger WIG craft to assess its longitudinal stability and dynamic motions can be found in (Chun and Chang, 2002). Tavakoli and Seif (2015) also investigated the longitudinal stability of a WIG craft using a potential-based theory. Because cases of extreme ground effects are not investigated in this study, wake roll-up is not considered in the code system implemented to solve for the takeoff of a wing. Although two-dimensional wings may have two Degrees of Freedom (2-DOF), pitching motion is not included in the study; instead, only heaving motion is considered. Heaving airfoils were investigated in (Liang *et al*., 2014), which analyzed forced and self-excited oscillations. Pitching motion, an important factor in assessing the longitudinal stability of craft and extreme ground effects, was investigated by Yang *et al*. (2012). Heave and pitch motions of a wing with zero-thickness in ground proximity was investigated by (Matveev, 2012) using potential theory. One-dimensional inviscid model adopted in his study is able to generate results both for flat and wavy grounds using linear and nonlinear theories.

Further improvements for WIG crafts in terms of wing efficiency can be made by twisting a three-dimensional wing in ground proximity. Studies made by Kinaci (2013) and Boschetti *et al*. (2008) investigate possible enhancements on wing geometry by giving it a twist at its ends. Utilization of a Power Augmented Ram (PAR) which aids the craft during takeoff is investigated in (Yang and Yang, 2010; Yang and Yang, 2011).

2 Mathematical background

Potential theory is implemented in this study to solve for the flow around a wing-in-ground effect. Although viscous effects may play a substantial role especially in extreme ground effect cases, this is not in the scope of this study. Viscous effects may still be superposed into potential theory by an "adaptive viscous-inviscid interaction method" as proposed by Rostami *et al*. (2016).

2.1 Dynamics of the motion of a wing

Newton's second law of motion dictates that

$$F' = \frac{\mathrm{d}(mV)}{\mathrm{d}t} \tag{1}$$

Consider a wing with a constant mass m which is flying with velocity U and clearance h above the ground, as shown in Fig. 1. The wing will be subjected to an aerodynamic force F exerted by the surrounding fluid and gravitational force mg that will act on its center of gravity. If it is assumed that the wing has 1-DOF and can only move vertically with velocity v. Keeping this in mind, Eq. (1) becomes

$$F + mg = m\frac{\mathrm{d}v}{\mathrm{d}t} \tag{2}$$

Rearranging and integrating Eq. (2) to solve for v and then integrating again to obtain the vertical displacement, we get

$$v = \int\left(\frac{F}{m} + g\right)\mathrm{d}t \tag{3}$$

$$y = \iint\left(\frac{F}{m} + g\right)\mathrm{d}t\mathrm{d}t \tag{4}$$

If the mass and force exerted by the fluid on the wing are known, Eqs. (3) and (4) are numerically solvable by setting the time step size to a reasonable value within a finite difference scheme. Force F is calculated by

$$F = \frac{1}{2}\rho c U^2 C_l \tag{5}$$

where c is the chord length and C_l is the lift coefficient of the wing. Using the Kutta–Joukowsky theorem, the lift coefficient can be calculated by

$$\begin{aligned} L = \rho U\Gamma &= \frac{1}{2}\rho c U^2 C_l \\ C_l &= \frac{2\Gamma}{cU} \end{aligned} \tag{6}$$

where Γ is the circulation around the wing. Here, it should be mentioned that the velocity U is independent of time. The problem handled in this study is a quasi-transient problem, and the wing is not starting from rest. The main focus is to determine the steady operating height; in other words, both the chord length c and velocity U in Equation 6 are constant, and C_l is a function of the circulation Γ only.

As is widely known, circulation is found by the equation

$$\Gamma = \int_{S_B} u_t \mathrm{d}s \tag{7}$$

where u_t is the tangential velocity at each infinitely small surface element ds of the wing integrated across the surface S_B. Tangential velocities over the wing are calculated by taking the derivative of the potential φ:

$$u_t = s_x\frac{\partial\varphi}{\partial x} + s_y\frac{\partial\varphi}{\partial y} \tag{8}$$

where the potential at each point is

$$\varphi = Ux + \mu \tag{9}$$

where μ is the doublet strength at every point in the fluid domain, including wing boundaries, which is solved for using the Boundary Element Method (BEM). The effect of the ground will be represented using the method of images. The auxiliary methods used in this study are briefly explained below.

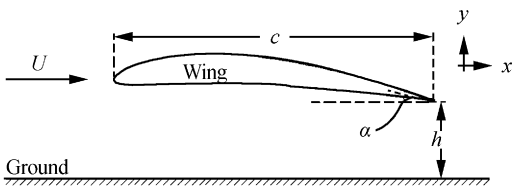

Fig. 1 Wing in ground proximity

2.2 BEM

The Laplace equation used to solve an inviscid flow is

given as

$$\nabla^2 \Phi = 0 \tag{10}$$

Green's identity gives a general solution of the Laplace equation as a sum of source and doublet distributions along a two-dimensional surface defined as

$$\Phi(x,y) = -\frac{1}{2\pi}\int_{S_B}\left[\sigma \ln r - \mu \frac{\partial}{\partial n}(\ln r)\right]\mathrm{d}S - \frac{1}{2\pi}\int_{S_W}\mu \frac{\partial}{\partial n}(\ln r)\mathrm{d}S + \Phi_\infty(P) \tag{11}$$

The doublet strengths μ for each point are found from Eq. (11). However, the solution for a lifting flow such as a wing in a ground effect is not unique, and the solution set is an overdetermined system. To overcome this problem, the Kutta condition is implemented at the trailing edge of the wing. A detailed explanation of this method and its parameters can be found in (Katz and Plotkin, 1991). The implementation of the iterative version of the method is given in the next section.

2.3 Method of images

A single wing can be solved by the direct implementation of BEM; however, the case with the ground below the wing changes the approach to the solution. The ground can be replaced by a mirror symmetrical reflection of the wing and air, and the problem can be solved as if there were two wings in the flow (Fig. 2). This method proves its worth by allowing the application of the computational benefits of IBEM.

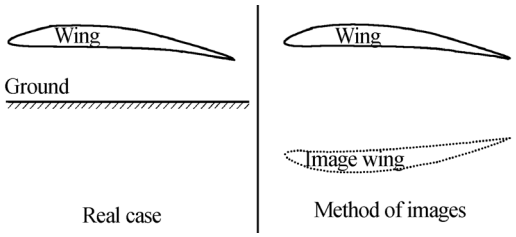

Fig. 2 Method of images

3 Solution approach

3.1 Mainstream of the developed code system

Two stand-alone sub-codes that communicate with each other through a mother code are developed to model the takeoff simulation. The first sub-code solves the flow around a wing and calculates the exerted aerodynamic force. The second sub-code calculates the vertical velocity of the wing and the displacement at each time step. The mother code is a batch file that commands the respective stand-alone sub-codes to work in order and transfers the results produced by each sub-code to the other. Fig. 3 illustrates the functioning of the batch file.

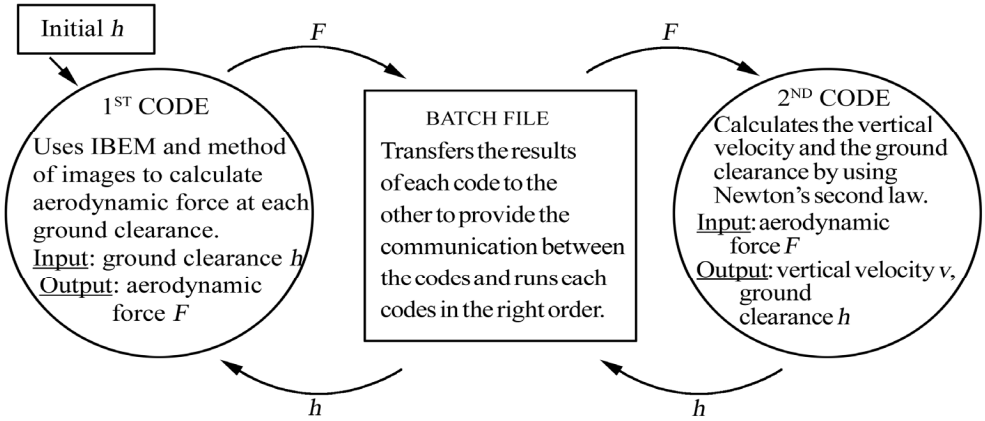

Fig. 3 Diagram of the functionalities of the stand-alone sub-codes and the role of the batch file

The method consists of the following steps:

1) Determine the doublet distribution along a wing using the IBEM implemented by the 1st sub-code.

2) Find tangential velocities along the surface of the wing using Eq. (8).

3) Calculate the circulation around the wing using Eq. (7).

4) Derive the lift coefficient of the wing using Eq. (6).

5) Calculate the vertical force on the wing using Eq. (5).

6) Calculate the vertical component of the wing's velocity using Eq. (3) implemented by the 2nd sub-code.

7) Calculate the vertical displacement through the finite difference scheme using Eq. (4) implemented by the 2nd sub-code.

8) Using the new ground clearance, return to step 1) for a new time step. Stop the iteration after the velocity difference between two consecutive time steps is less than a prescribed value.

The vertical velocity of the wing will theoretically be equal to zero at its peak position. The wing will continue to operate at the same height until there is any intervention. The code system will exit the iterative loop after the difference between the velocities of consecutive time steps is lower than 10^{-4}.

To start the procedure, doublet strengths along the surface of a wing that is in ground proximity should be found. A guide as to how these are calculated is given in Section 3.2.

Steps 2)–5) are straight forward and can be calculated using equations provided in Section 2 (Eqs. (5) through (8)). Steps 6) and 7) use the finite difference scheme to calculate vertical displacements; the numerical approach to solve these steps is given in Section 3.3.

3.2 Calculation of aerodynamic force—1st sub-code

The aerodynamic force on the wing is calculated by the IBEM. As shown in previous studies (Bal, 2008; Kinaci, 2014; Kinaci, 2015), the IBEM is faster than BEM and produces accurate results. The solution steps of IBEM implementation by the sub-codes are as follows:

1) Solve the flow around a real wing as if it alone is in the flow and find doublet strengths along its surface.

2) Solve the flow around an imaginary wing using potentials induced by the real wing and find doublet strengths along its surface.

3) Solve the flow around the real wing using potentials induced by the imaginary wing and find doublet strengths along its surface.

4) Return to step 2) and continue as an iterative process. Stop when the difference in doublet strengths between two consecutive iterations is less than $\varepsilon=10^{-5}$, where ε is the prescribed value, that stops the iterative process. It is defined as

$$\varepsilon = \mu_i - \mu_{i-1} \tag{12}$$

where μ_i is the doublet strength calculated at each iteration on an arbitrary panel. Converged doublet strengths are used in the 1st step of the mother code.

3.3 Calculation of vertical velocity and displacement—2nd sub-code

1st order finite difference method is implemented to numerically solve Eqs. (3) and (4) for the vertical velocity and displacement, respectively. These equations become

$$\Delta v = \frac{F_t \cdot \Delta t}{m} - g \cdot \Delta t \tag{13}$$

$$y_{t+1} = y_t + \Delta v \cdot \Delta t \tag{14}$$

The calculations of the vertical velocity and displacement are performed using steps 6) and 7) of the mother code. The displacement obtained in the 2nd sub-code is used as an input for the 1st sub-code.

4 Validation of the IBEM code

The code system was validated against the experimental results of Ahmed and Sharma (2005) for the NACA0015 wing; a comparison is presented in Fig. 4. As observed in the figure, the general trends of curves agree, although some discrepancies are found between the respective results. The code system returns higher values than the experimental results. As mentioned previously, the code system uses the IBEM to generate its results and thus relies on potential theory; because potential theory completely neglects the effect of fluid velocity, the resulting values obtained in this study are higher than the experimental results.

As shown in Fig. 4, the difference between the results increases as the AoA increases. The greatest discrepancy occurs when AoA is 10° because viscosity affects bluff bodies more than streamlined bodies. The effect of viscosity on bluff bodies is very high,and surpassing a specific AoA, it makes will cause a wing to go into stall and lose lift owing to the effects of the separation of the flow at the suction side of the wing. The IBEM implementing potential theory cannot detect this phenomenon. Qu *et al*. (2014) investigated the incidence of flow separation on a model WIG craft using CFD.

Differences between pressure distributions at the suction side of a wing obtained in the present study and the experimental work of Ahmed and Sharma (2005) can be clearly observed in Fig. 5. Although there appears to be a significant difference at the suction side, the IBEM returns more accuratere sults for the pressure side of the wing. It is easily apparent from Fig. 5 that the IBEM returns lower pressure values. Once again, this is caused by potential theory discounting the pressure caused by viscous effects. The existence of viscous pressure in the experimental case limits the obtained values for lift. In contrast, the higher lift predictions in this study stem from an inviscid flow assumption. Further investigation of the effects of viscosity on a wing in ground proximity was performed by Yang *et al*. (2010), and another experiment using the NACA0015 wing can be found in Luo and Chen (2012).

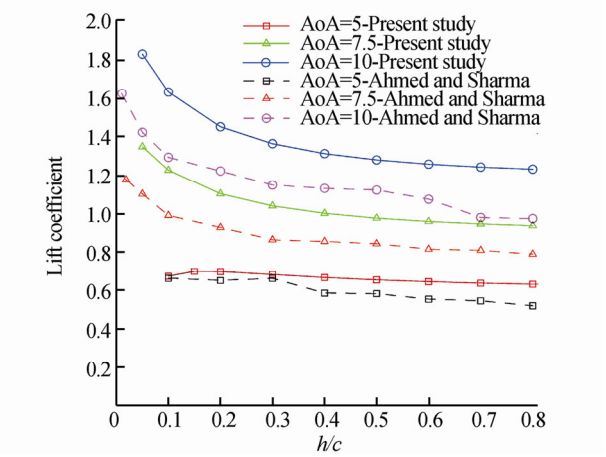

Fig. 4 Comparison of C_l from the present study with that from the study by Ahmed and Sharma (2005)

5 Takeoff of an NACA6409 wing using the model

It is reported in the previous section that potential theory neglects viscosity, returning higher values for lift generation of the wing. However, the IBEM is still successful in grasping the working principles of the ground effect, and the general trends of the respective curves agree (see Figs. 4 and 5). The IBEM and potential theory can be utilized to predict the force acting on a wing to simulate the takeoff of the wing in proximity to the ground.

In this section, the takeoff of a two-dimensional

NACA6409 wing that is initially at rest over the ground is solved using the model proposed in this study. The wing is actually not touching the ground because this would ruin the structure of the numerical model; instead, it is very close to the ground. To prevent any numerical errors that might arise, the wing is assumed to be located only 0.01c above the ground. The parameters used in this study are given in Table 1.

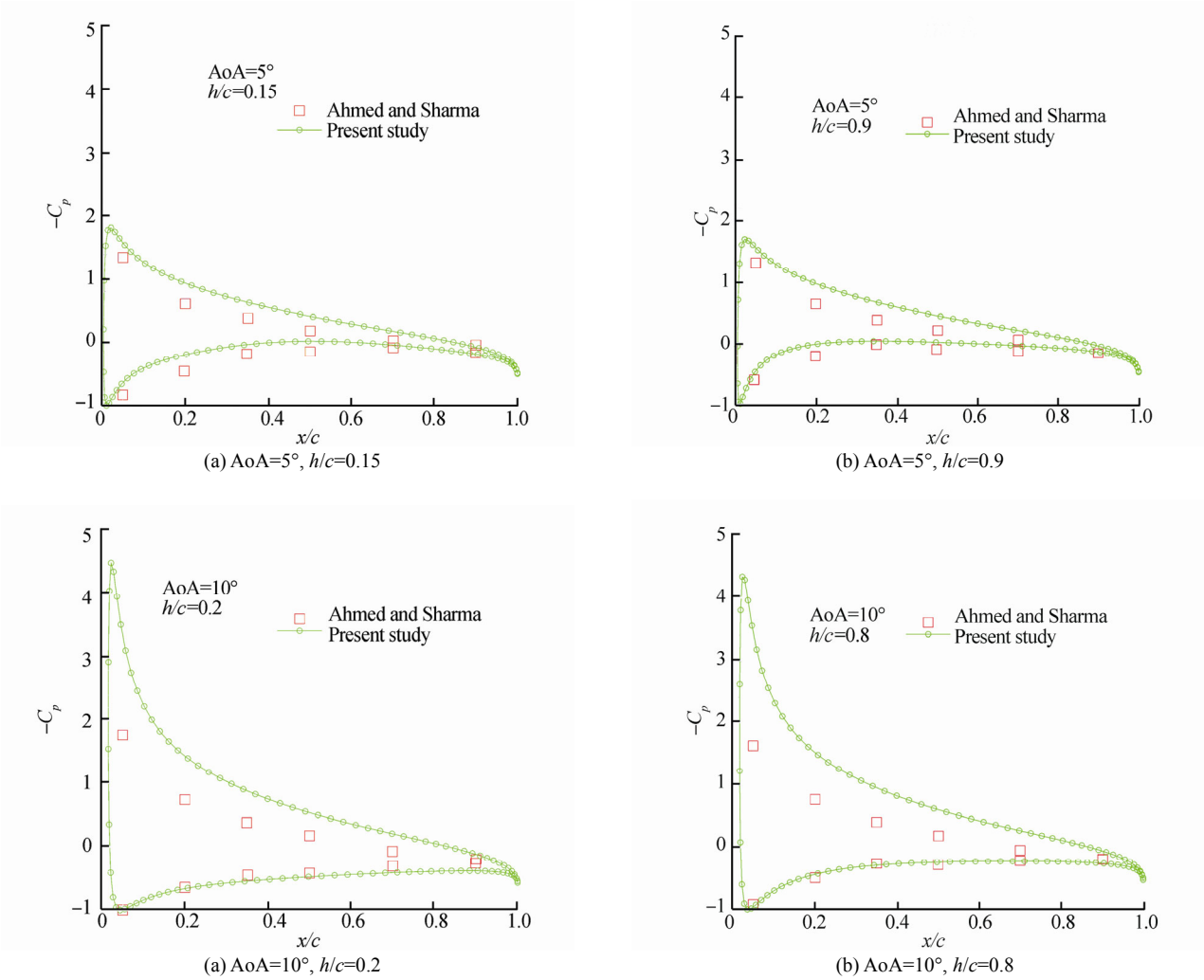

(a) AoA=5°, h/c=0.15 (b) AoA=5°, h/c=0.9

(a) AoA=10°, h/c=0.2 (b) AoA=10°, h/c=0.8

Fig. 5 Comparison of C_p distributions from the present study with those from the study by Ahmed and Sharma (2005)

Table 1 Parameters used in this study to model takeoff

Wing profile	NACA6409
Angle of attack α/(°)	4
Chord length of the wing c/m	1
Free-stream velocity V/(m·s^{-1})	1
Fluid density ρ/(kg·m^{-3})	1.225
Mass of the wing m/kg	0.087 5
Time step size Δt/s	0.1
Gravity g/(m·s^{-2})	9.81

Clearance from the ground, velocity, and force with respect to time are given in Figs. 6, 7, and 8, respectively. When close to the ground, a wing experiences a greater aerodynamic force exerted on it owing to increased pressure at the pressure side. The wing rises with a high velocity and the ground clearance increases rapidly during takeoff. As the wing moves away from the ground, the aerodynamic force exerted on the wing substantially decreases. This decrease results in a slower takeoff velocity and smaller vertical displacement. After a sufficient amount of time, the wing reaches its operating height. When there is a small amount of displacement between time steps, the force applied to the wing remains about the same, and the WIG reaches a steady state. At Ut/c=6.7, when the wing reaches the operating height, the vertical velocity of the wing should be less than the prescribed value $\varepsilon \leq 10^{-4}$ because there should be no significant vertical displacement after the wing reaches the operating height.

To understand what happens to the wing over time, the pressure distribution along its surface is observed. Non-dimensionalized pressure distributions along the surface of the wing at Ut/c=0, Ut/c=1 and Ut/c=6.7 are

shown in Fig. 9.

The pressure at the pressure side of the wing is much higher at the initial condition when the wing is close to the ground. The pressure starts to decrease as it moves further away from the ground, and the pressure change during the first second is much higher than that during the following seconds, which explains why the aerodynamic force shown in Fig. 8 drops significantly following the start. There is also some change in the suction side of the wing, but this change is much smaller than that at the pressure side.

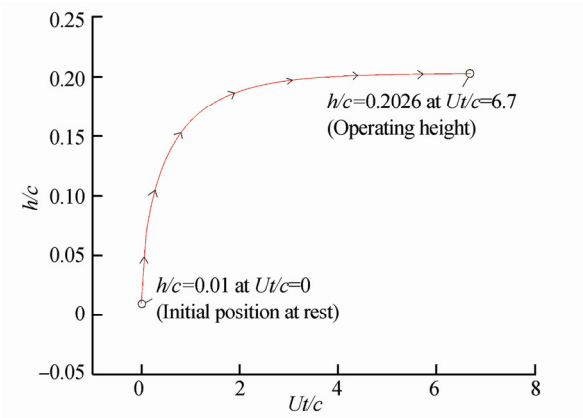

Fig. 6 Elevation of the WIG from the ground as a function of time following takeoff

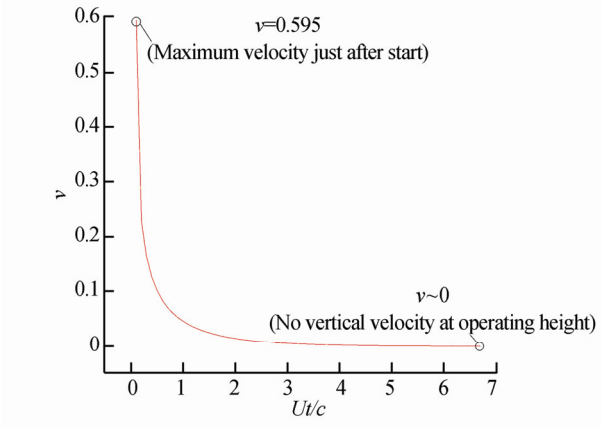

Fig. 7 Velocity during takeoff

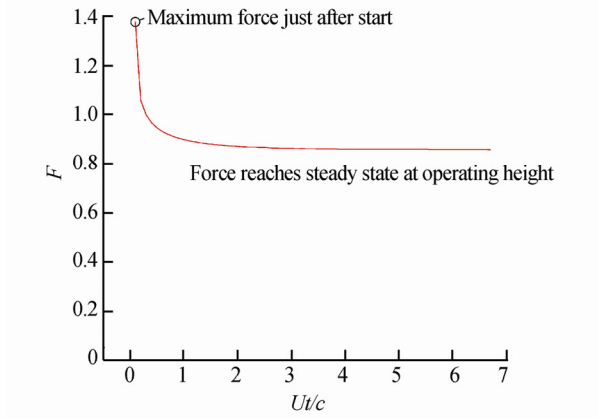

Fig. 8 Force applied to the WIG over time

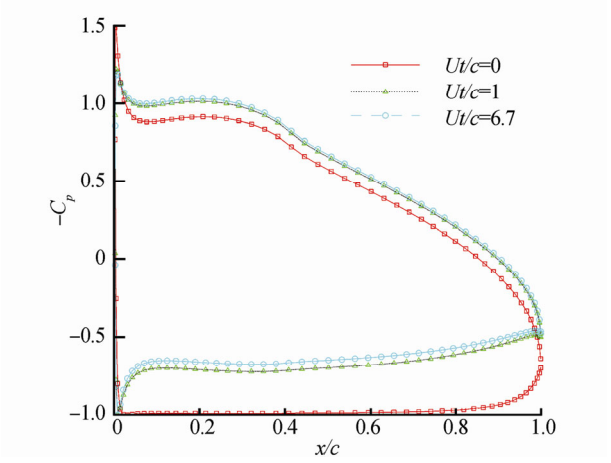

Fig. 9 Non-dimensional pressure distribution change overtime

6 Effects of thickness and AoA of a wing

6.1 Effect of thickness

The effects of thickness of a wing on takeoff and operating height are investigated in this section. For this purpose, takeoffs of NACA6408 and NACA6410 wings are solved using the proposed model and compared with the ascent of a NACA6409 wing. The ground clearance with respect to time is given in Fig. 10. Thinner wings have lower operating heights but reach peak before thicker wings, which is an expected result as it is previously known that thickness has a positive effect on lift generation; this in turn results in a greater aerodynamic force. The pressure distributions of the wings are compared at their peak levels in height in Fig. 11. Except at the leading edge of the suction side of the wing, the pressure on thicker wings is lower; this is the main reason why thicker wings generate higher lift.

6.2 Effect of AoA

The effect of AoA effect on takeoff is investigated by changing the α of the NACA6409 wing by ±1°. The ground clearance with respect to time is given in Fig. 12, and pressure coefficient distributions along the wing at their peak level are given in Fig. 13. As shown in these figures, as the AoA of the wing increases, the wing can operate at increasing ground clearances. A low AoA can reach the peak level in a shorter time but can only operate at a lower height. Changes in AoA also affect the pressure distribution along the wing. A smaller AoA causes the wing to work under higher pressures for which the pressure difference between the suction and pressure sides is much lower when compared with higher AoA wings. The pressure difference leads to more lift generation, higher aerodynamic force, and increased operating height. As AoA increases, pressure significantly decreases in the suction side at the leading edge of the wing. The pressure difference between two consecutive points at this part of the wing is also important as it can lead to boundary layer separation on the wing. Because the IBEM implements potential theory and does not consider viscosity, the developed code system cannot detect

stall. As the effects of stall are likely to cause problems during flight, this phenomenon must be kept in mind while increasing AoA.

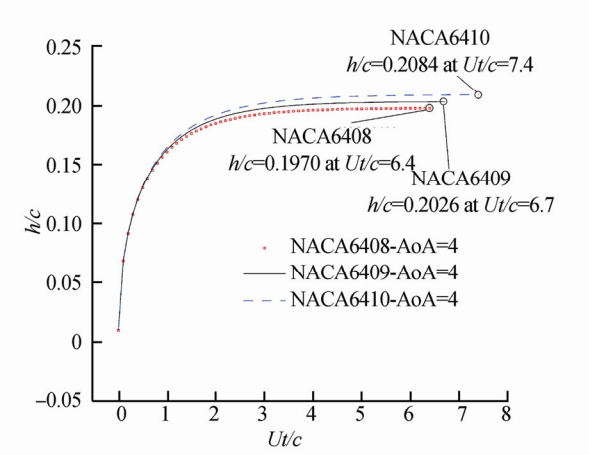

Fig. 10 Effect of thickness on takeoff

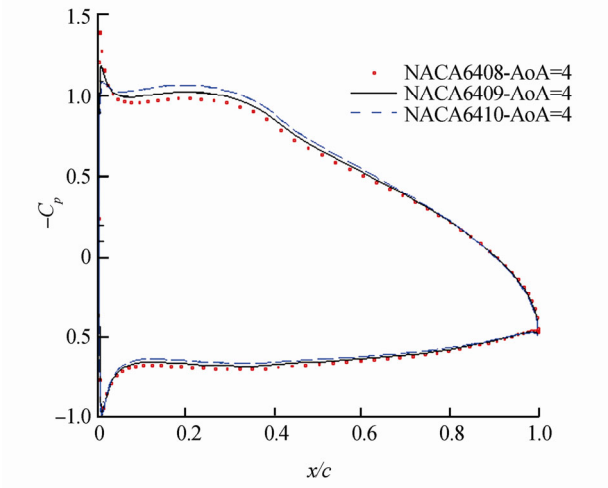

Fig. 11 Pressure coefficient distribution around different geometries at peak positions

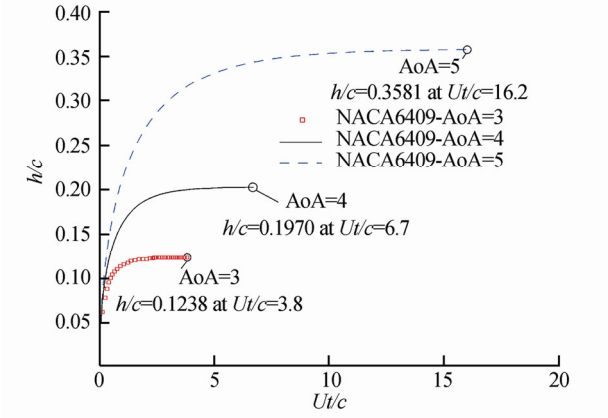

Fig. 12 Effect of AoA on takeoff

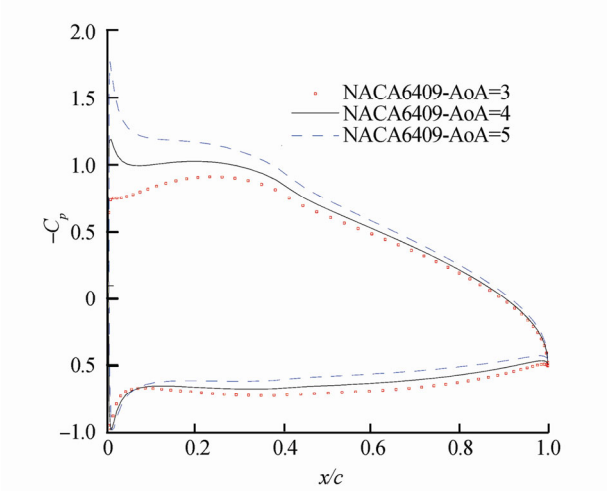

Fig. 13 Pressure coefficient distribution around different AoAs at peak positions

7 Conclusions

A mathematical model to calculate the flight dynamics of wings in proximity to the ground was developed in this study. The method uses the IBEM to calculate the aerodynamic force on the wing. Although the model is also applicable to RANSE-based solutions, the IBEM is much faster than RANSE and provides a practical method to assess wings at the pre-design stage of a WIG craft. RANSE may be useful at later stages when the geometry of a wing is specified and a need to improve the accuracy of results arises.

Using the model, the takeoff of an NACA6409 wing that is initially at rest was simulated, and graphs of the aerodynamic force, velocity, and clearance from the ground were plotted. The change in pressure distribution along a wing over time was observed. The effects of thickness and AoA were investigated. The major findings in this study are as follows:

1) Thicker wings can operate at higher clearances but reach operating height later.

2) The AoA of a wing significantly changes the operating height.

3) The pressure difference at the suction side of the leading edge of a wing increases with AoA. High pressure differences between two consecutive points can cause a wing to stall earlier.

Pitching motion, which is very important to the longitudinal stability of a wing, was not assessed in this study. The proposed mathematical model and code system may be developed futher to consider both the pitching and heaving motions of a wing.

References

Ahmed MR, Sharma SD, 2005. An investigation on the aerodynamics of a symmetrical airfoil in ground effect. *Experimental Fluid and Thermal Sciences*, **29**(6), 633-647. DOI: 10.1016/j.expthermflusci.2004.09.001

Bal S, 2008. Prediction of wave pattern and wave resistance of surface piercing bodies by a boundary element method. *International Journal for Numerical Methods in Fluids*, **56**(3), 305-329.
DOI: 10.1002/fld.1527

Bal S, Kinnas SA, 2002. A BEM for the prediction of free surface effects on cavitating hydrofoils. *Computational Mechanics*, **28**(3-4), 260-274.
DOI: 10.1007/s00466-001-0286-7

Barber TJ, 2007. A study of water surface deformation due to tip vortices of a wing-in-ground effect. *Journal of Ship Research*, **51**(2), 182-186.

Boschetti, PJ, Cardenas EM, Amerio A, 2008. Increasing the lift-drag ratio of an unmanned aerial vehicle using local twist. *Journal of Aircraft*, **45**(1), 10-15.
DOI: 10.2514/1.33353

Chun HH, Chang CH, 2002. Longitudinal stability and dynamic motions of a small passenger WIG craft. *Ocean Engineering*, **29**(10), 1145-1162.
DOI: 10.1016/S0029-8018(01)00098-1

Halloran M, O'Meara S, 1999. *Wing in ground effect craft review*. DSTO Aeronautical and Maritime Research Laboratory, Melbourne, 14.

Katz J, Plotkin A, 1991. *Low speed aerodynamics-from wing theory to panel methods*. Mc-Graw Hill Inc., Singapore, 52-87.

Kinaci OK, 2013. Effect of wing twist in ground proximity. *FAST2013*, Amsterdam, Netherlands.

Kinaci OK, 2014. An iterative boundary element method for a wing-in-ground effect. *International Journal of Naval Architecture and Ocean Engineering*, **6**(2), 282-296.
DOI: 10.2478/IJNAOE-2013-0179

Kinaci OK, 2015. A numerical parametric study on hydrofoil interaction in tandem. *International Journal of Naval Architecture and Ocean Engineering*, **7**(1), 25-40.
DOI: 10.1515/ijnaoe-2015-0003

Kinnas SA, Fine NE, 1993. A numerical nonlinear-analysis of the flow around 2-dimensional and 3-dimensional partially cavitating hydrofoils. *Journal of Fluid Mechanics*, **254**, 151-181.
DOI: 10.1017/S0022112093002071

Liang H, Wang X, Zou L, Zong Z, 2014. Numerical study of two-dimensional heaving airfoils in ground effect. *Journal of Fluids and Structures*, **48**, 188-202.
DOI: 10.1016/j.jfluidstructs.2014.02.009

Liang H, Zong Z, 2011. A subsonic lifting surface theory for wing-in-ground effect. *Acta Mechanica*, **219**(3-4), 203-217.
DOI: 10.1007/s00707-011-0444-8

Luo SC, Chen YS, 2012. Ground effect on flow past a wing with a NACA0015 cross-section. *Experimental Thermal and Fluid Sciences*, **40**, 18-28.
DOI: 10.1016/j.expthermflusci.2012.01.014

Matveev KI, 2012. Heave-pitch motions of a platform flying in extreme ground effect. *Journal of Aerospace Engineering*, **25**(2), 238-245.
DOI: 10.1061/(ASCE)AS.1943-5525.0000126

Nebylov AV, 2003. *Controlled WIG flight – Stability and efficiency problems*. PhysCon 2003, Saint Petersburg, Russia.

Qu Q, Lu Z, Liu P, 2014. Numerical study of aerodynamics of a wing-in-ground effect craft. *Journal of Aircraft*, **51**(3), 913-924.
DOI: 10.2514/1.C032531

Rostami AB, Ghadimi P, Ghassemi H, 2016. Adaptive viscous-inviscid interaction method for analysis of airfoils in ground effect. *Journal of the Brazilian Society of Mechanical Sciences and Engineering*, (published online).
DOI: 10.1007/s40430-016-0485-y

Rozhdestvensky KV, 2006. Wing-in-ground effect vehicles. *Progress in Aerospace Sciences*, **42**(3), 211-283.
DOI: 10.1016/j.paerosci.2006.10.001

Tavakoli M, Seif MS, 2015. A practical method for investigation of aerodynamic and longitudinal static stability of wing-in-ground effect. *International Journal of Maritime Technology*, **3**(4), 11-19.

Uslu Y, Bal S, 2008. Numerical prediction of wave drag of 2-D and 3-D bodies under or on a free surface. *Turkish Journal of Engineering and Environmental Sciences*, **32**(3), 177-188.

Yang W, Lin F, Yang Z, 2012. Investigation on application of high-lift configuration to wing-in-ground effect. *Proceedings of the Institution of Mechanical Engineers, Part G: Journal of Aerospace Engineering*, **226**(G3), 260-271.
DOI: 10.1177/0954410011409488

Yang W, Yang Z, 2011. Schemed power-augmented flow for wing-in-ground effect craft in cruise. *Chinese Journal of Aeronautics*, **24**(2), 119-126.
DOI: 10.1016/S1000-9361(11)60015-0

Yang W, Yang Z, Collu M, 2015. Longitudinal static stability requirements for wing in ground effect vehicle. *International Journal of Naval Architecture and Ocean Engineering*, **7**(2), 259-269.
DOI: 10.1515/ijnaoe-2015-0018

Yang Z, Yang W, 2010. Complex flow for wing-in-ground effect craft with power augmented ram engine in cruise. *Chinese Journal of Aeronautics*, **23**(1), 1-8.
DOI: 10.1016/S1000-9361(09)60180-1

Yang Z, Yang W, Jia Q, 2010. Ground viscous effect on 2D flow of wing in ground proximity. *Engineering Applications of Computational Fluid Mechanics*, **4**(4), 521-531.